Nano-structure study of ZnO thin films on sapphire grown with different temperature conditions

Shu-Cheng Chin[a], Chun-Yung Chi[a], Yen-Cheng Lu[a], Lin Hong[a], Yu-Li Lin[a], Fang-Yi Jen[a], C.C. Yang[a],*, Bao-Ping Zhang[b], Yusaburo Segawa[b], Kung-Jen Ma[c], Jer-Ren Yang[d]

[a]Graduate Institute of Electro-Optical Engineering and Department of Electrical Engineering, National Taiwan University, 1, Roosevelt Road, Sec. 4, Taipei, Taiwan, ROC
[b]Photodynamics Research Center, RIKEN (the Institute of Physical and Chemical Research), Sendai, Japan
[c]Department of Mechanical Engineering, Chung Hua University, Hsinchu, Taiwan, ROC
[d]Department of Material Science and Engineering, National Taiwan University, Taipei, Taiwan, ROC

Abstract

We compared the nano-structures of three samples of ZnO thin film on sapphire under different growth temperature conditions. Although disconnected domain structures (on the scale of 100 nm in size) were observed in the samples of high-temperature (450 °C) growth, their crystal quality is generally better than the one grown at a low temperature (200 °C), either near or away from the sapphire interface. Lattice misfits and threading dislocations were observed within a domain with the separation of around 8 nm. The sample grown at the low temperature showed a continuous structure through the ZnO layer although void-like structures might exist inside. However, its crystal quality is relatively poorer. Of the two samples with high-temperature growth, the one with initial low-temperature growth had a larger domain structure (around 150 nm in size) and relatively lower crystal quality. In particular, strong strains existed near the interface of this sample. The samples of high-temperature growth generally have higher photon emission efficiencies. Temperature-dependent integrated photoluminescence intensities of the high-temperature-growth samples show that the exciton trapping by either intrinsic donors or acceptors leads to a higher thermal quenching rate in comparison with free excitons.
© 2006 Elsevier B.V. All rights reserved.

1. Introduction

Because of its large exciton binding energy at about 60 meV, ZnO has attracted much attention in crystal growth and optical property studies. With such a large exciton binding energy, the dominance of exciton recombination in the radiative process, even up to the room temperature, results in the high photon emission efficiency for device application. Recently, significant progresses in ZnO crystal quality have been made. Besides the nano-structures like nano-tubes [1], nano-rods [2], and nano-walls [3], high-quality ZnO thin films have been grown with molecule-beam epitaxy [4,5], metal-organic chemical vapor deposition (MOCVD) [6,7], and sputtering [8].

In ZnO, because of the existence of Zn interstitials and O vacancies, and the substitution of O by Zn, effective shallow donors are usually formed [9]. A donor can trap an electron to form a neutral donor. A neutral donor can trap a free exciton (FX) to form a donor-bound exciton (D^0X). Also, because of the existence of O interstitials and Zn vacancies, effective deep acceptors can be formed [10]. A neutral acceptor, which is generated after an acceptor receives a hole, can trap a FX to form an acceptor-bound

---

*Corresponding author. Tel.: +886 2 23657624; fax: +886 2 23652637.
E-mail address: ccy@cc.ee.ntu.edu.tw (C.C. Yang).

exciton (A^0X). Normally, the donor density is higher than the acceptor density in a high-quality ZnO sample. Another widely observed emission feature in ZnO is the donor–acceptor pair (DAP) [11]. This emission feature is due to the combination of an electron trapped by a donor and a hole trapped by an acceptor. Because the donor level is quite shallow from the conduction band edge, the DAP transition level can be easily thermalized into the conduction band-neutral acceptor transition level (symbolized by eA^0) as temperature increases [12]. At medium temperatures, the DAP emission feature coincides with the emission feature of one-LO-phonon-assisted emission, which is about 70 meV (LO phonon energy) below the FX level [13].

The nanostructures of ZnO heavily rely on the MOCVD growth conditions, particularly on the growth temperature and pressure [6,8,14–17]. By decreasing the growth pressure, the ZnO nanostructures change from nano-rods into nano-tubes and then nano-walls. ZnO nano-rods, nano-tubes, and nano-walls are normally obtained at 10–6, 1–0.3, and 0.1–0.06 Torr, respectively, in growth pressure [16,17]. In the growth temperature dependence, when the growth temperature is lower than 250 °C, smooth surfaces without grain formation were observed [15]. The migration of atoms on the substrate surface is suppressed at low growth temperatures. However, when the growth temperature is higher, zinc atoms become more diffusive on the substrate surface. They can select sites having smaller lattice mismatch. When the growth temperature is higher than 300 °C in growing ZnO on sapphire, we can normally observe that the unit cell of ZnO is twisted in the c-plane by 30° with respect to that of sapphire (Al_2O_3) [15]. In this situation, high-quality growth can be achieved with a lower density of misfit dislocation.

In this paper, we use the technique of high-resolution transmission electron microscopy (HRTEM) for studying the nanostructures of three ZnO thin-film samples, grown on sapphire, of different growth temperature conditions. It is found that generally the crystalline quality is higher in the sample grown at the high temperature through the whole growth procedure. The basic optical measurements show that higher photon emission efficiency can also be obtained with the high growth temperature. This paper is organized as follows: In Section 2, we describe the sample growth conditions and the HRTEM operation conditions. The surface morphologies of the samples are also discussed here. Then, in Section 3, we present and discuss the images of HRTEM of these samples. The results of basic optical characterization are shown in Section 4. Finally, conclusions are drawn in Section 5.

2. Sample preparation and research approaches

All the three ZnO thin-film samples were grown with MOCVD on (0 0 0 1) sapphire substrate with 6 Torr in pressure. Sample A was grown at 450 °C for 90 min. In this sample, measurements by using X-ray diffraction (XRD)

revealed that the in-plane orientation of ZnO unit cell is 30° twisted relative to that of the sapphire substrate [15]. Sample B was grown at 200 °C for 90 min. In this sample, the in-plane orientation of ZnO unit cell is not twisted. Sample C was grown at 200 °C for 5 min first, followed by 90-min growth at 450 °C. In this situation, the in-plane orientation of ZnO unit cell is not twisted either. The HRTEM investigations were performed using a Philips Tecnai F30 field-emission electron microscope using an acceleration voltage of 300 kV and a probe forming lens of $Cs = 1.2$ mm. The current density focused onto the samples was estimated to be lower than 16 A/cm^2.

Figs. 1–3 show scanning electron microscopy (SEM) images of samples A–C, respectively. In Fig. 1 for sample A, which was grown at the high temperature, spiral domain
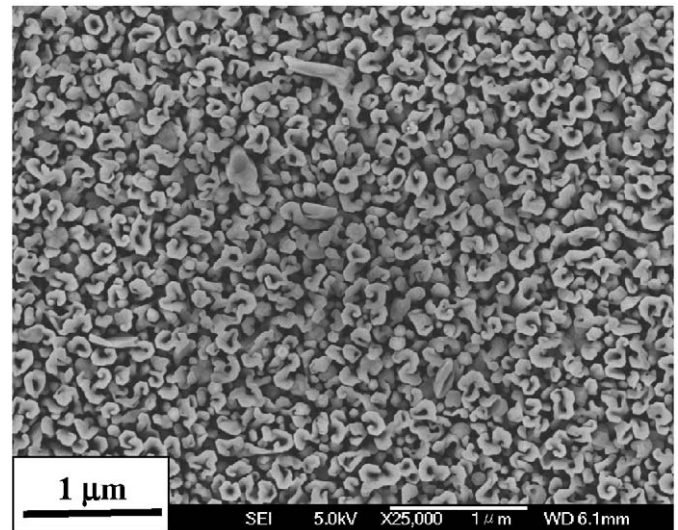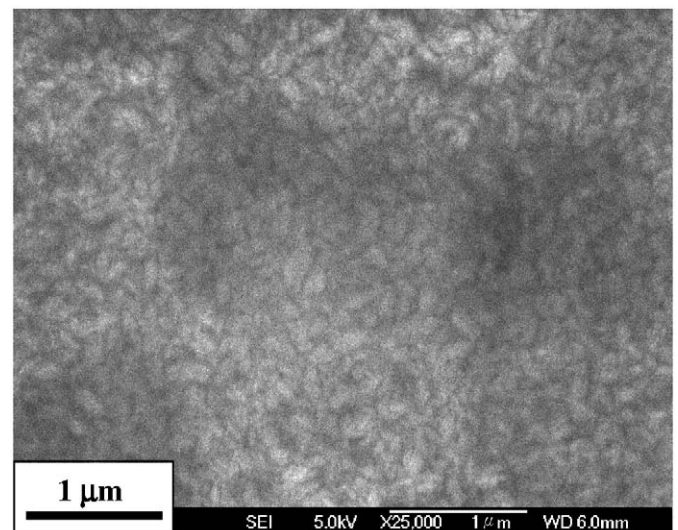

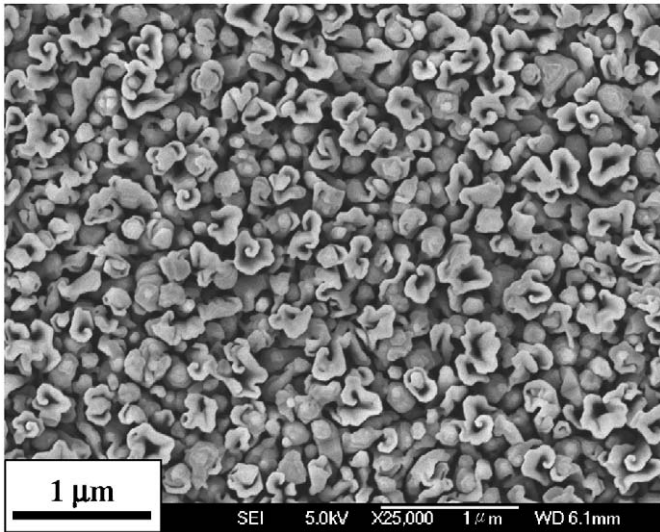Fig. 1. An SEM image of sample A.

Fig. 2. An SEM image of sample B.

Fig. 3. An SEM image of sample C.

structures with a scale size of 100 nm can be seen. The ZnO thin film is actually composed of random domain structures and air gaps. The surface morphology looks like a mixture of flowers in full blossom and flower buds. However, in Fig. 2 for sample B, which was grown at the low temperature, although domain structures can be seen, they seem to be well connected. Then, in Fig. 3 for sample C, which was initially grown at the low temperature, followed by the high-temperature growth, spiral domain structures similar to those in sample A (a mixture of flowers in full blossom and flower buds) can be observed. Nevertheless, the domain structures are larger in scale size (around 150 nm), when compared with sample A.

3. Images of transmission electron microscopy (TEM)

Fig. 4 shows a large-scale TEM image of sample A. Here, one can clearly see that the thin film actually consists of separate domain structures that are consistent with the surface morphology shown in Fig. 1. The cross section of a domain is around 100 nm in size. The domains seem to be mutually separated starting from the ZnO/sapphire interface. Fig. 5 shows an HRTEM image around the ZnO/sapphire interface of sample A. The interface is quite clear. Generally speaking, the ZnO crystalline quality is high. It is noted that although atomic point image can be seen in the sapphire layer, only line structures are seen in the ZnO layer. This difference indicates the different crystal orientations between the two layers, confirming that the ZnO basal plane is twisted by 30°. Fig. 6 shows a typical HRTEM image in the shallow layer of ZnO. Here, two threading dislocations along the c-axis with the separation of about 8 nm can be clearly seen. Except the threading dislocations, the crystalline quality of ZnO is actually quite good. Because of the large lattice mismatch between sapphire and ZnO, threading dislocations can be found along the interface. Such a structure can be seen in Fig. 7.
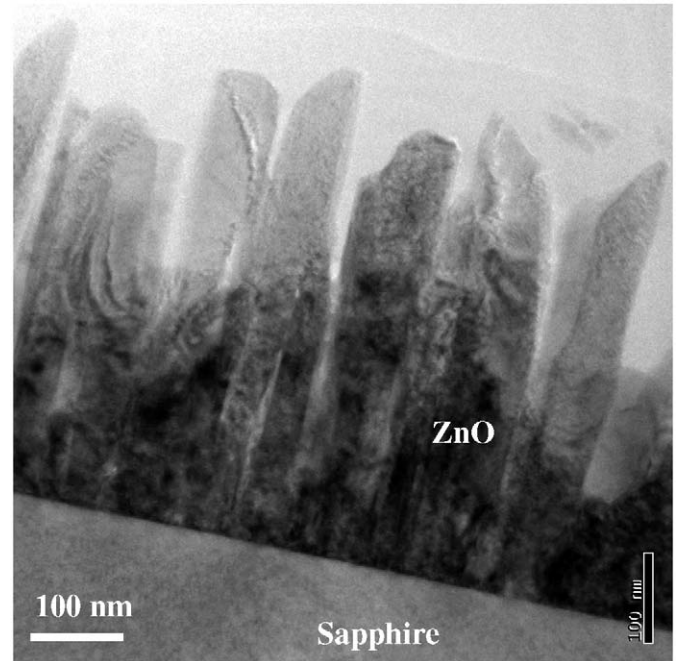

Fig. 4. A large-scale TEM image of sample A showing the domain structures. The domain size is around 100 nm.
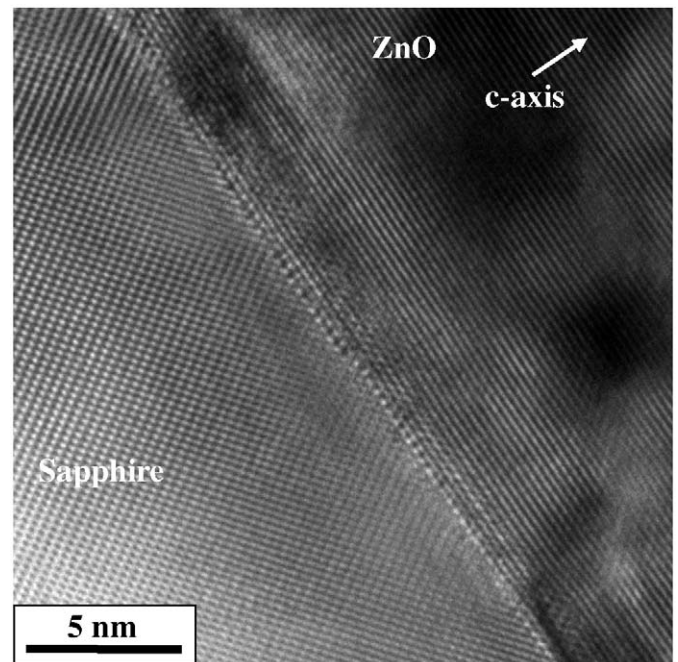

Fig. 5. A TEM image showing the interface between the sapphire substrate and ZnO of sample A.

As indicated with arrows, three threading dislocations can be seen in this HRTEM image. The separation between two neighboring dislocations is about 8 nm. A misfit dislocation exists in this range for releasing the built strain. Such a threading dislocation extends along the ZnO growth in the c-axis. It is noted that the 30° twist of the ZnO basal plane, relative to the sapphire crystalline, has reduced the
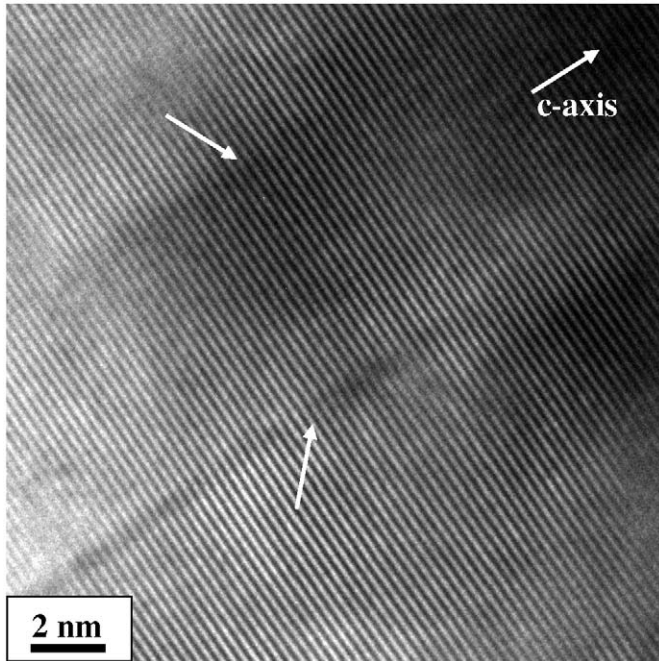
Fig. 6. A TEM image showing the ZnO structure of sample A. Two threading dislocations separated by about 8 nm can be seen.
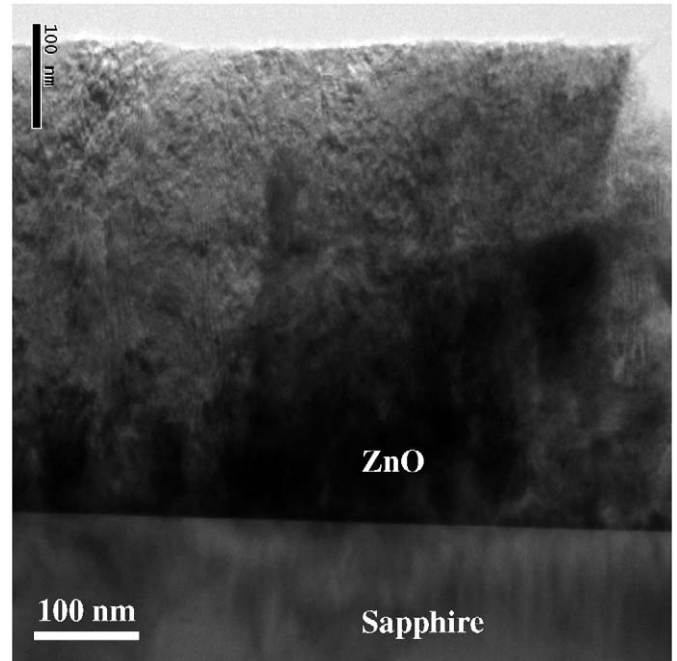

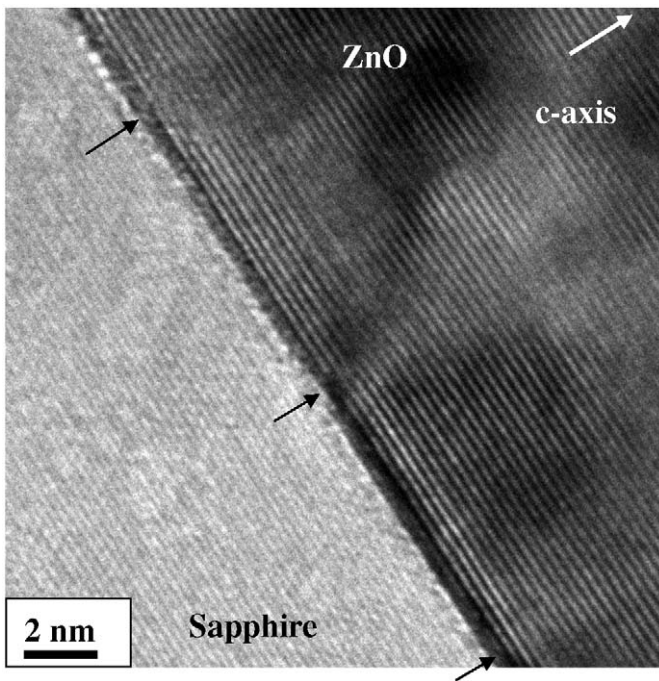Fig. 8. A large-scale TEM image of sample B.

Fig. 7. Another TEM image showing the interface between sapphire substrate and ZnO of sample A. The marked points indicate the starting points of three threading dislocations.
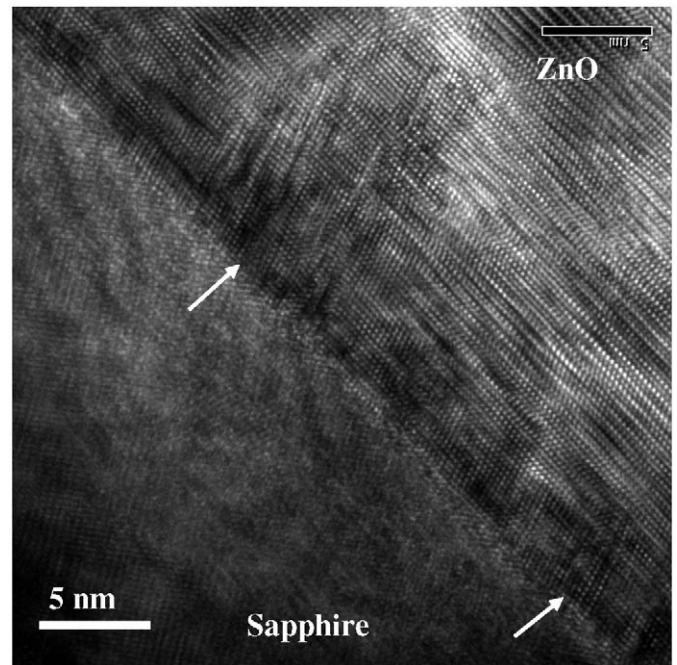

Fig. 9. A TEM image showing the interface between the sapphire substrate and ZnO of sample B. The stacking faults in ZnO indicate the strong strain distribution near the interface.

lattice mismatch between ZnO and sapphire from 31.5% to 18.3% [15]. Although it is difficult to calibrate the correspondence between the 18.3% lattice mismatch and the observed 8-nm separation of threading dislocation, this distance can be interpreted as the extent of strain the system can stand before the bond breakage and the

formation of misfit dislocations. Without the 30° basal-plane twist, the dislocation density may become higher.

Fig. 8 shows a large-scale TEM image of sample B. Here, a continuous layer of ZnO of about 500 nm in thickness can be seen. This continuous structure is consistent with the surface morphology in Fig. 2 and is quite different from that of sample A. Fig. 9 shows the atomic-scale image at the interface between the sapphire substrate and ZnO of

sample B. Here, the atomic dot images for both sapphire and ZnO can be seen, confirming that the crystal orientation of ZnO is not twisted with respect to sapphire. Basically, the interface is clear although not as sharp as that in sample A. However, plenty of stacking faults can be seen in ZnO near the interface, indicating that strong strains are distributed in this region. It has been discussed that a twist of crystal orientation in the basal plane of the hexagonal structure can relax the strain energy [18]. In the case of low-temperature growth, the incorporated atoms do not have sufficient thermal energy for forming the twisted structure such that the built strains are stronger in sample B. In Fig. 9, two regions of line structures oriented about 75° with respect to the interface can also be seen. Such line structures represent the misfit defects for relaxing the lattice mismatch-built strains.

Fig. 10 shows a large-scale TEM image of sample C. Near the top, domain structures similar to those of sample A can be observed. However, the scale size along the interface dimension is larger, on the order of 150 nm. This observation is again consistent with the surface morphology, as shown in Fig. 3. Also, from Fig. 10 one can see that the domain structures in sample C are actually connected near the interface, similar to the case of sample B. This observation is reasonable because in the first 5 min of growth for sample C, the growth temperature was 200 °C, the same as that for the whole growth process of sample B. Fig. 11 shows an image near the interface of sample C. Here, one can see that the ZnO crystalline quality near the interface is quite poor, similar to the case of sample B. Line structures like those in sample B can also be observed. Here, again the observable atomic dot matrices in both
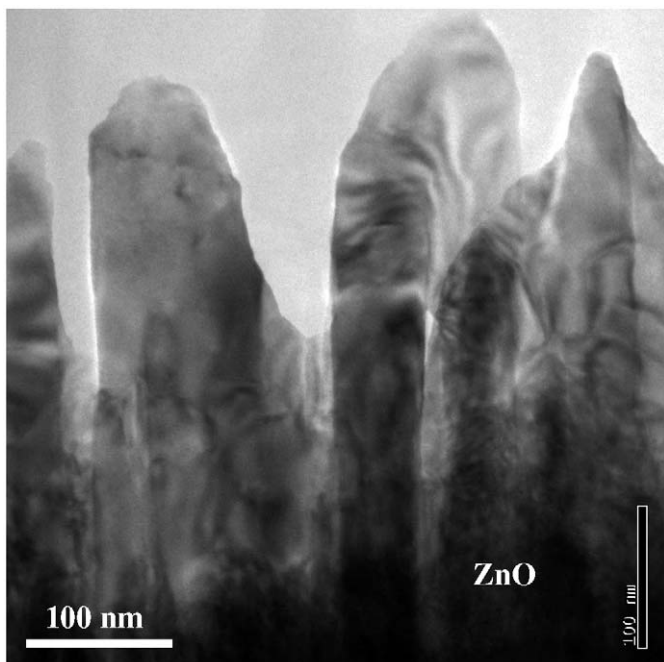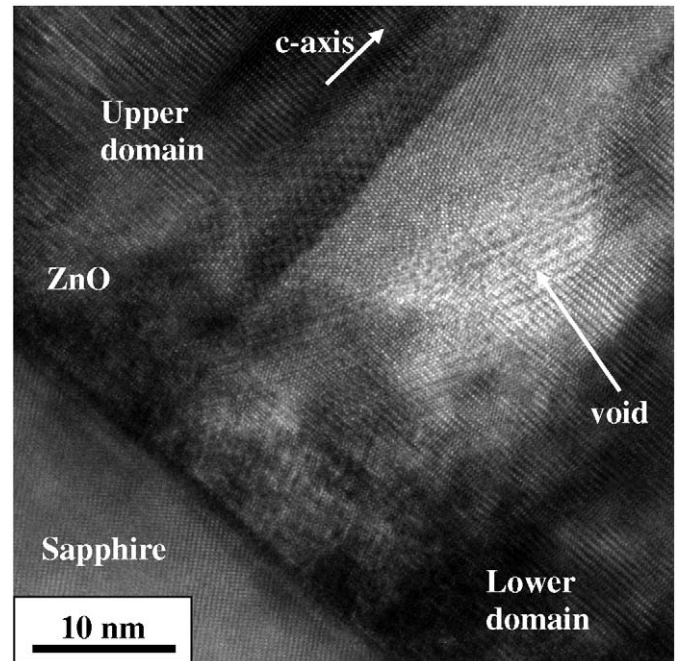

Fig. 11. A TEM image showing the interface between the sapphire substrate and ZnO of sample C.

sapphire and ZnO confirm that the ZnO crystalline is not twisted in the basal plane with respect to sapphire in sample C.

Note that although a void-like structure exists between the upper and lower domains in Fig. 11, the atomic arrangement essentially connects the two domains near the interface. Because the growth condition of this region is the same as that of the whole growth process of sample B, the observed void-like structure can be used for explaining the blurred domain structures of sample B, as shown in Fig. 2. Void-like structures could be generated during the low-temperature growth. Such a void-like structure near the interface may become the seed of the domain gap between two evolving domains when the growth temperature is elevated to 450 °C. Here, one can see the sharp boundary between the upper domain and the gap. However, the smooth transition between the lower domain and the gap can be observed. It is difficult to clearly determine the boundary of the lower domain. This image may demonstrate a spiral structure, in which the crystalline portion of the lower domain extends gradually away from the HRTEM focal point and then returns to the focal point to show the upper domain. The gap in Fig. 11 may correspond to the crystalline portion away from the focal point. In sample C, the atomic-scale image of the ZnO layer near the top surface (not shown in this paper) shows that except a few lines of stacking faults, the ZnO crystalline structure is quite good in the high-temperature growth portion.

The domain structures formed with the high-temperature growth are attributed to the higher growth speed of ZnO along the c-axis. It is more likely to implement the

Fig. 10. A large-scale TEM image of sample C showing the domain structures. The domain width is around 150 nm.

2-D growth mode at the low temperature. In this situation, however, void-like structures may exist and the crystalline quality is relatively poorer.

4. Basic optical properties

In Figs. 12 and 13, we show the temperature-dependent photoluminescence (PL) spectra of samples A and C, respectively. The PL intensity of sample B is too weak to be measured with our equipment indicating the poor optical quality of this sample that is consistent with the results of material analysis. In Fig. 12 for sample A, at 10 K the peak near 3.36 eV corresponds to D^0X. That near 3.37 eV beyond 40 K corresponds to FX. Also, the evolving peak

Fig. 12. PL spectra of sample A at various temperatures.

Fig. 13. PL spectra of sample C at various temperatures.

around 3.3 eV beyond 60 K is due to the contributions of DAP and one-LO-phonon-assisted FX emission. Below 40 K, excitons are mainly trapped by neutral donors. Because of the thermal energy, excitons are thermalized into free states to form the FX peak beyond 40 K. This peak becomes dominating and starts to red shift due to the thermal effect beyond 80 K. In the thermal effect, lattice vibration weakens the bond strength and reduces the band gap of the semiconductor. Beyond 140 K, the thermal energy is larger than the binding energy of a neutral donor and hence FX and D^0X become mixed. When the temperature approaches the room temperature, the complex of FX and D^0X mix with the contributions of DAP and one-LO-phonon-assisted FX emission. In this situation, DAP may be thermalized into the state of eA^0. The PL behaviors in Fig. 12 were commonly observed in high-quality ZnO samples [19].

The PL behaviors in Fig. 13 for sample C are rather different. At 10 K, besides the minor peak near 3.36 eV of D^0X, there is a broad major peak around 3.325 eV. This peak may cover the possible contribution of DAP near 3.3 eV at 10 K. It can also be attributed to the increase of the A^0X density [20]. The effective deep acceptor defects are mainly due to the existence of O interstitials and Zn vacancies in the sample. It is speculated that the low-temperature (low-quality) growth in the initial stage of sample C led to a higher acceptor density in the shallow layer, which is the major sample portion of the PL measurement, although the higher temperature was used in the later-stage growth. At low temperatures, the excitons are trapped by the deep-level neutral acceptors. Beyond 80 K, they are mainly thermalized into D^0X and then FX. Eventually, FX emission dominates at room temperature. The existence of the acceptor feature indicates the major difference in material structure between samples A and C. Although it requires further investigation, based on the comparison between samples A and C, the low-temperature initial-growth stage seems to increase the acceptor density.

In Fig. 14, we show the integrated PL intensities as functions of temperature for samples A and C. The decay rate of the integrated PL intensity is usually used to describe the density of non-radiative recombination center in a sample. The steeper decay with increasing temperature of sample C implies that the density of non-radiative recombination centers in this sample is higher than that of sample A. It is noted that the thermal quenching process of the integrated PL intensity in sample A shows a turning point at 80 K, beyond which the quenching rate is reduced. From Fig. 14, one can see the coincidence with the temperature of the emergence of FX. Also, a similar turning point exists at 120 K for sample C. From Fig. 13, one can see that this temperature corresponds to the point that the A^0X emission becomes less important and FX begins to dominate. Based on such an observation, one can conclude that the trapping of excitons by neutral donors or acceptors may create a channel of non-radiative
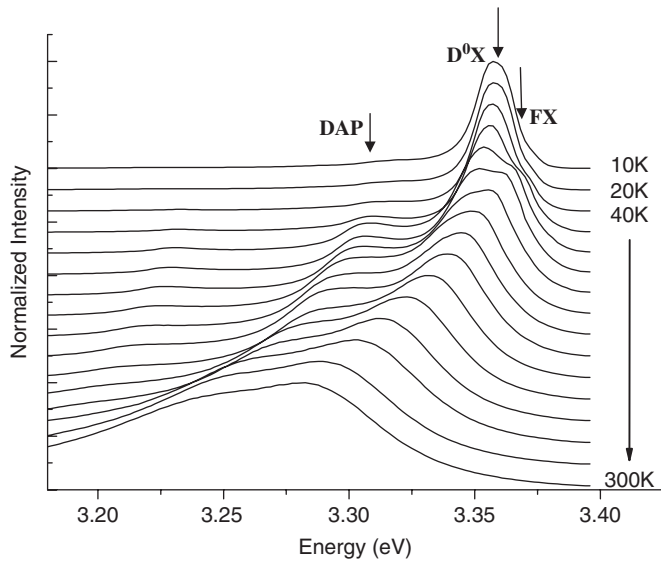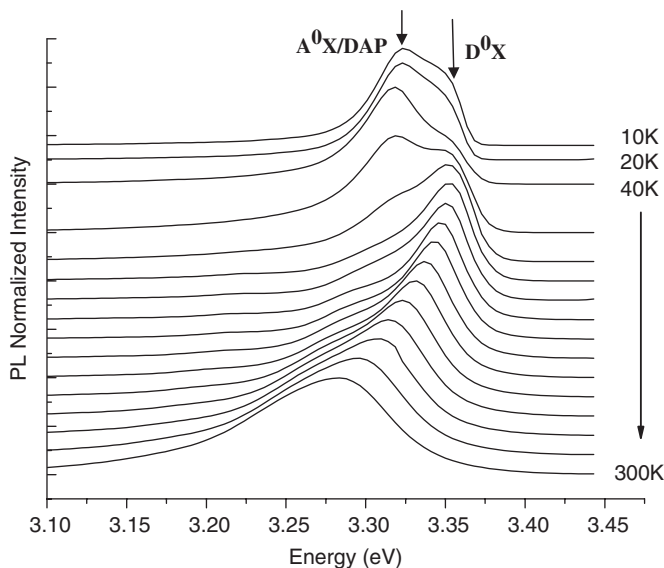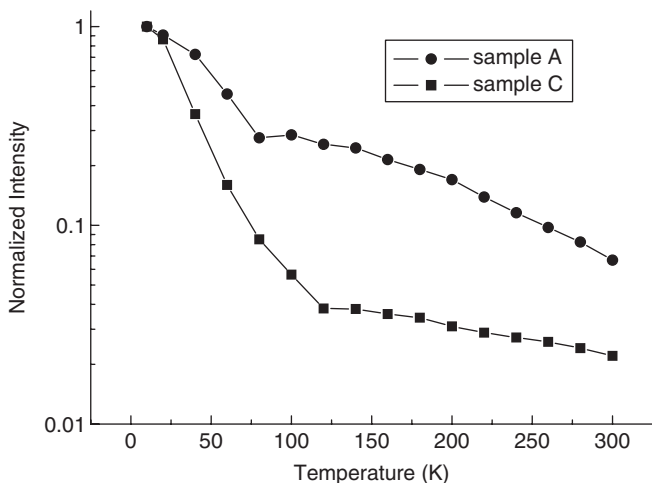
Fig. 14. Integrated PL intensities as functions of temperature of samples A and C.

integrated photoluminescence intensities of the high-temperature-growth samples, one could conclude that the exciton trapping by either intrinsic donors or acceptors leads to a higher thermal quenching rate in comparison with free excitons.

recombination. Excitons may relax from the defect levels through phonon generation. As temperature increases to provide thermal energy for ionizing excitons from the defect trapping to become FXs, the thermal quenching rate is reduced. Therefore, beyond 80 K for sample A and beyond 120 K for sample B, the decay slopes of the integrated PL intensities of samples A and C become shallower.

5. Conclusions

In summary, we have compared the nano-structures of three ZnO thin films grown on sapphire under different growth temperature conditions. Although disconnected domain structures were observed in the samples of high-temperature growth, their crystal quality was generally better than the one grown at the low temperature. Lattice misfits and threading dislocations were observed within a domain with the separation of about 8 nm. The sample grown at the low temperature showed a continuous structure through the ZnO layer although void-like structures might exist inside. However, its crystal quality was relatively poorer. Of the two samples with high-temperature growth, the one with initial low-temperature growth had a larger domain structure and relatively lower crystal quality. In particular, strong strains existed near the interface of this sample. The samples of high-temperature growth generally had higher photon emission efficiencies. From the observation of the temperature-dependent

References

[1] X.W. Sun, S.F. Yu, C.X. Xu, C. Yuen, B.J. Chen, S. Li, Jpn. J. Appl. Phys. 42 (2003) 229.
[2] W.I. Park, Y.H. Jun, S.W. Jung, G. Yi, Appl. Phys. Lett. 82 (2003) 964.
[3] H.T. Ng, J. Li, M.K. Smith, P. Nguyen, A. Cassell, J. Han, M. Meyyappan, Science 300 (2003) 1249.
[4] Y. Chen, D. Bagnall, T. Yao, Mater. Sci. Eng. B 77 (2000) 190.
[5] D.C. Look, D.C. Reynolds, C.W. Litton, R.L. Jones, D.B. Eason, G. Cantwell, Appl. Phys. Lett. 81 (2002) 1830.
[6] K. Haga, T. Suzuki, Y. Kashiwaba, H. Watanabe, B.P. Zhang, Y. Segawa, Thin Solid Films 433 (2003) 131.
[7] T. Gruber, C. Kirchner, K. Thonke, R. Sauer, A. Waag, Phys. Stat. Sol. (a) 192 (2002) 166.
[8] S.F. Chichibu, T. Yoshida, T. Onuma, H. Nakanishi, J. Appl. Phys. 91 (2002) 874.
[9] B.P. Zhang, N.T. Binh, K. Wakatsuki, C.Y. Liu, Y. Segawa, N. Usami, Appl. Phys. Lett. 86 (2005) 032105.
[10] B. Guo, Z.R. Qiu, K.S. Wong, Appl. Phys. Lett. 82 (2003) 2290.
[11] Q.X. Zhao, M. Willander, R.E. Morjan, Q.H. Hu, E.E.B. Campbell, Appl. Phys. Lett. 83 (2003) 165.
[12] B.P. Zhang, N.T. Binh, Y. Segawa, K. Wakatsuki, N. Usami, Appl. Phys. Lett. 83 (2003) 1635.
[13] K.I. Ogata, T. Kawanishi, K. Maejima, K. Sakura, S. Fujita, Jpn. J. Appl. Phys. 40 (2001) 657.
[14] Th. Gruber, C. Kirchner, K. Thonke, R. Sauer, A. Waag, Phys. Stat. Sol. (a) 192 (2002) 166.
[15] B.P. Zhang, K. Wakatsuki, N.T. Binh, N. Usami, Y. Segawa, Thin Solid Films 449 (2004) 12.
[16] S. Muthukumar, H. Sheng, J. Zhong, Z. Zhang, N.W. Emanetoglu, Y. Lu, IEEE Trans. Nanotechnol. 2 (2003) 50.
[17] B.P. Zhang, N.T. Binh, K. Wakatsuki, Y. Segawa, Y. Yamada, N. Usami, M. Kawasaki, H. Koinuma, J. Phys. Chem. B 108 (2004) 10899.
[18] B.P. Zhang, N.T. Binh, K. Wakatsuki, N. Usami, Y. Segawa, Appl. Phys. A 78 (2004) 25.
[19] O. Pagni, G.R. James, A.W.R. Leitch, Phys. Stat. Sol. (c) 1 (2004) 864.
[20] H. Kato, M. Sano, K. Miyamoto, T. Yao, Jpn. J. Appl. Phys. 42 (2003) 2241.